UNIVERSITY OF LEEDS

White Rose
university consortium
Universities of Leeds, Sheffield & York

eprints@whiterose.ac.uk
https://eprints.whiterose.ac.uk/

Improved Realtime State-of-Charge Estimation of LiFePO$_4$ Battery Based on a Novel Thermoelectric Model

Cheng Zhang, Kang Li, *Senior Member*, *IEEE*, Jing Deng, and Shiji Song

Abstract—Li-ion batteries have been widely used in electric vehicles, and battery internal state estimation plays an important role in the battery management system. However, it is technically challenging, in particular, for the estimation of the battery internal temperature and state-of-charge (SOC), which are two key state variables affecting the battery performance. In this paper, a novel method is proposed for realtime simultaneous estimation of these two internal states, thus leading to a significantly improved battery model for realtime SOC estimation. To achieve this, a simplified battery thermoelectric model is firstly built, which couples a thermal submodel and an electrical submodel. The interactions between the battery thermal and electrical behaviours are captured, thus offering a comprehensive description of the battery thermal and electrical behaviour. To achieve more accurate internal state estimations, the model is trained by the simulation error minimization method, and model parameters are optimized by a hybrid optimization method combining a meta-heuristic algorithm and the least square approach. Further, time-varying model parameters under different heat dissipation conditions are considered, and a joint extended Kalman filter is used to simultaneously estimate both the battery internal states and time-varying model parameters in realtime. Experimental results based on the testing data of LiFePO$_4$ batteries confirm the efficacy of the proposed method.

Index Terms—Internal temperature estimation, SOC estimation, thermoelectric model, joint extended Kalman Filter

I. INTRODUCTION

ELECTRIC vehicles (EVs) and hybrid electric vehicles (HEVs) have gained rapid development worldwide in recent years as a means to tackle the pollutions and low efficiency problems of internal combustion engine based vehicles in the transportation sector. The EV and HEV batteries usually consist of hundreds or even thousands of battery cells connecting in series/parallel configuration. Therefore, a battery management system (BMS) is essential to ensure safe and efficient battery operations [1]. One key functionality of the BMS is to estimate battery internal states that are not directly measurable, such as the battery internal temperature and state of charge (SOC) which are two major factors affecting the battery performance.

In practice, only the surface temperature is directly measurable for commercially used EV batteries. Yet, it is the battery internal temperature that directly affects the battery performance, and a large temperature difference may occur between battery internal and surface temperatures (e.g., sometimes greater than $10°C$ [2]), especially in high power demand applications. Realtime estimation of the battery internal temperature is thus of great importance for BMS. Firstly, high internal temperature is a real threat to battery safe operation [1]. Excessive temperature can greatly accelerate the battery ageing process, and even cause fire or explosion of the battery pack in severe cases [3]. The battery internal temperature can reach to a critical temperature a lot quicker than the surface temperature, thus the surface temperature measurement alone is not sufficient to ensure safe battery operation. Secondly, the battery electrical properties, such as usable capacity, internal resistance and power delivery ability all depend on the battery internal temperature. Therefore, it can help develop a more accurate battery electrical model by estimating the battery internal temperature. Finally, the estimation of the battery internal temperature can serve as an indicator in designing proper battery thermal management strategies.

Over the years, various battery thermal models of different accuracy and complexity levels have been proposed, such as complex distributed electrochemical thermal models for thermal simulation [4], [5] and simplified lump-parameter thermal models for realtime applications [6], [7]. Based on the developed models, different model-based estimation methods, such as Kalman filter method, have been proposed for realtime estimation of the battery internal temperature [8], [9].

Battery SOC is another key indicator for EV and HEV batteries. Battery SOC indicates the charge left in the battery available for further service, and it is like the fuel gauge in an ICE car, thus inaccurate SOC estimation may cause the car to strand halfway. Besides, battery SOC can also be used to prevent over-charging and over-discharging operations. There are various SOC estimation methods available in the literature [10]–[14].

Cheng Zhang, Kang Li and Jing Deng are with the School of Electronics, Electrical Engineering and Computer Science, Queen's University Belfast, 125 Stramillis Road, Ashby Building, Belfast, BT9 5AH, UK. Email: czhang07@qub.ac.uk; k.li@qub.ac.uk; dengjing101@gmail.com
Shiji Song is with Department of Automation, Tsinghua University, Beijing 100084, China; E-mail: shijis@mail.tsinghua.edu.cn

Despite extensive researches have been carried out, to our knowledge, few papers have dealt with the simultaneous realtime estimation of both the battery internal temperature and SOC, though these two states are closely coupled. Further, for model based battery internal state estimation methods, a battery model needs to be built first. Yet, few papers have considered the interactions between the battery internal thermal and electrical behaviours, except for those complex three dimensional electrochemical models [15], [16]. However, these first-principle electrochemical models are not suitable for realtime EV applications. On the other hand, many papers on battery SOC estimation did consider the effect of the ambient temperature on battery electrical performance [17]–[19], but only the battery surface temperature is used.

In our previous work [20], the estimation of the battery internal temperature is addressed based on a novel simplified battery thermoelectric model, based on which SOC is then estimated. While the proposed model in [20] has a good model accuracy, but when it is used for the SOC estimation, the results are still poor in some cases. Further, in [20], only heat generation from the series internal resistance is considered, and the model is only applicable for natural heat convection condition at room temperature. The effect of forced heat dissipation methods, which are commonly used in the battery thermal management system, on the battery thermal behaviour is not studied.

The main contributions of this paper are summarized as follows. Firstly, methods for estimating the heat generation rate inside the battery, a key element for building a suitable battery thermal model are investigated and compared. Secondly, time-varying parameters in the thermal model under different heat dissipation conditions are taken into consideration to achieve higher modelling accuracy. Thirdly, a more realistic and detailed battery electrical model that considers both the battery relaxation effect and hysteresis effect is adopted. The battery electrical model is identified under different SOC and temperature levels. With the above introduced techniques, the effect of battery internal temperature and SOC on the battery electrical behaviours is thus captured in detail, offering a comprehensive and better description of the battery thermal and electrical behaviours. Fourthly, to improve the model accuracy, the simulation error minimization method is adopted for training the battery model, and a hybrid optimization method that combines a meta-heuristic algorithm (i.e., the teaching learning based optimization (TLBO) method) and the least square approach is adopted for model parameter optimization. Finally, a joint extended Kalman filter method is applied to estimate the internal model states and time-varying model parameters simultaneously.

The rest of this paper is organized as follows. Section II presents a simplified battery thermoelectric model, including an electrical submodel and a thermal submodel. The test data collected under different heat dissipation scenarios are discussed in Section III. The simulation error minimization model training method and the hybrid parameter optimization method are given in section IV, along with the identified model parameters and modelling results. Considering the time-varying nature of the model parameters, joint EKF method

is applied to estimate the battery internal states and the time-varying model parameters simultaneously in Section V. The experimental results are presented and analysed. Finally, Section VI concludes this paper.

II. BATTERY THERMOELECTRIC MODEL

A. Battery electric circuit model

Different kinds of battery models have been developed so far [21]. For the LiFePO$_4$ battery used in this paper, to achieve accurate modelling and state estimation, two key challenges must be addressed, i.e., the hysteresis effect and the long relaxation process. In this paper, we adopt a second-order electric circuit model coupled with the hysteresis effect as shown in Fig 1,
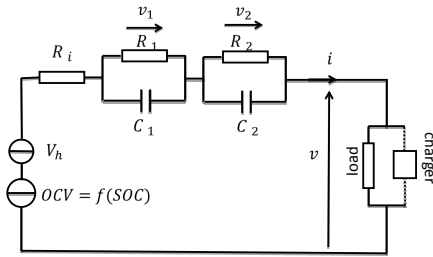

Fig. 1. Battery electric circuit model

where OCV is the battery open circuit voltage (OCV), v, i are the battery terminal voltage and current, respectively. R_i represents the battery internal resistance. R_1C_1 is used to capture the battery short-term relaxation dynamics, while R_2C_2 for capturing the long-term relaxation process. The over-potentials across these two RC networks are v_1, v_2, respectively. Battery OCV is the battery terminal voltage when the battery internal equilibrium is reached in the absence of load. Battery OCV depends on the battery SOC, temperature and previous charging/discharging history, which is referred to as the hysteresis effect and is captured by V_h. However, according to [22], battery OCV changes slowly with temperature, e.g., less than 10mV as temperature changes from -10 to $50°C$. Therefore, the temperature effect on battery OCV is not considered here, and

$$OCV = f(soc) \tag{1}$$

Battery SOC can be calculated as follows,

$$soc(k) = soc(k-1) + i(k-1) * T_s/3600/C_n \tag{2}$$

where T_s is the sampling time in seconds, and C_n is the battery nominal capacity in Ampere hour (Ah).

Following the dynamics of a RC network, we have

$$v_l(k) = a_l * v_l(k-1) + b_l * i(k-1) \tag{3}$$

where $a_l = exp(-T_s/R_l/C_l), b_l = R_l * (1 - a_l), l = 1, 2$.

The same battery hysteresis dynamic model proposed in [13] is adopted here, as follows,

$$V_h(k) = e^{-\gamma*|i(k-1)|} * V_h(k-1) +$$
$$(1 - e^{-\gamma*|i(k-1)|}) * sign(i(k-1)) * M_h \tag{4}$$
$$= c_{k-1} * V_h(k-1) + d_{k-1} * M_h$$

where M_h is the maximum hysteresis value, and γ adjusts the changing rate of V_h.

Combing Eq (1 - 4), the battery electrical submodel can be described as

$$x_e(k) = A_e(k-1) * x_e(k-1) + B_e(k-1) \qquad (5)$$

where

$$x_e(k) = [soc(k), v_1(k), v_2(k), V_h(k)]^T$$

and $A_e = diag([1, a_1, a_2, c_{k-1}])$, $B_e(k-1) = [i(k-1) * T_s/3600/C_n, b_1 * i(k-1), b_2 * i(k-1), d_{k-1} * M_h]^T$

According to Fig 1, battery terminal voltage, $v(k)$ can be calculated as,

$$v = OCV + V_h + R_i * i + v_1 + v_2 \qquad (6)$$

B. Battery thermal submodel

A battery thermal model consists of two parts: thermal generation and thermal transfer within and outside the battery. Although the heat generation inside the battery is a complex electrochemical process, to build a simplified battery thermal model, three different heat generation calculation methods are widely adopted [6]–[9], [23], i.e.,

$$\begin{aligned} Q_1 &= R_i * i^2 \\ Q_2 &= i * (v - OCV) \\ Q_3 &= i * (v - OCV) + i * T_{in} * \frac{dOCV}{dT_{in}} \end{aligned} \qquad (7)$$

while Q_1 only considers the heat generation over the battery internal resistance R_i; Q_2 considers the heat generation caused by the over-potentials such as v_1, v_2, V_h; Q_3 further takes into consideration of the heat generation due to entropy change within the battery [9].

Assume that the battery shell temperature and internal temperature are both uniform, and heat generation is uniformly distributed within the battery. Heat conduction is assumed to be the only heat transfer form between the battery internal and shell, and between the battery shell and the ambience.

The resulting simplified battery thermal submodel is given as follows,

$$\begin{aligned} C_{q1} * \frac{dT_{in}}{dt} &= Q_j - k_1 * (T_{in} - T_{sh}), \quad j \in \{1, 2, 3\} \\ C_{q2} * \frac{dT_{sh}}{dt} &= k_1 * (T_{in} - T_{sh}) - k_2 * (T_{sh} - T_{amb}) \end{aligned} \qquad (8)$$

where T_{in} and T_{sh} are battery internal and shell temperature, respectively; T_{amb} is the ambient temperature; C_{q1}, C_{q2} are the battery internal and shell thermal capacity, respectively; Q_j is the heat generation rate; k_1 and k_2 are the heat conduction coefficients between the battery internal and the shell, and between the battery shell and the ambience, respectively.

Eq (8) can be discretized and reformulated as

$$x_t(k) = A_t(k-1) * x_t(k-1) + B_t(k-1) \qquad (9)$$

where

$$x_t(k) = [T_{in}(k), T_{sh}(k)]^T$$

$$A_t = \begin{bmatrix} 1 - T_s * k_1/C_{q1} & T_s * k_1/C_{q1} \\ T_s * k_1/C_{q2} & 1 - T_s * (k_1 + k_2)/C_{q2} \end{bmatrix}$$

$$B_t(k-1) = [T_s/C_{q1} * Q_j(k-1), T_s/C_{q2} * k_2 * T_{amb}]^T$$

C. Coupled thermoelectric model

By combining Eq (5) and (9), the simplified thermoelectric model is given as follows,

$$\begin{aligned} x(k) &= A(k-1) * x(k-1) + B(k-1) \\ v(k) &= f(soc(k)) + V_h(k) + v_1(k) + v_2(k) + R_i * i(k) \end{aligned} \qquad (10)$$

where

$$x(k) = [x_e(k); x_t(k)]$$

$$A(k-1) = blkdiag(A_e(k-1), A_t(k-1))$$

$$B(k-1) = [B_e(k-1); B_t(k-1)]$$

Note that T_{sh} is a model state as well as a model output, since it is directly measurable.

III. TEST DATA

The test system includes a charger, an electric load and the temperature is controlled by a thermal cabinet, as shown in Fig 2. The Li-ion battery used in this paper is a prismatic LiFePO$_4$-Graphite battery purchased from the open market. The battery structure includes the outside shell, i.e., the battery can made of Aluminium, and the internal layers which can be further divided into three identical sub-cells connected in parallel. Two thermocouples are attached to the battery shell surface, and another thermocouple is inserted into the center area between sub-cell 1 and sub-cell 2.
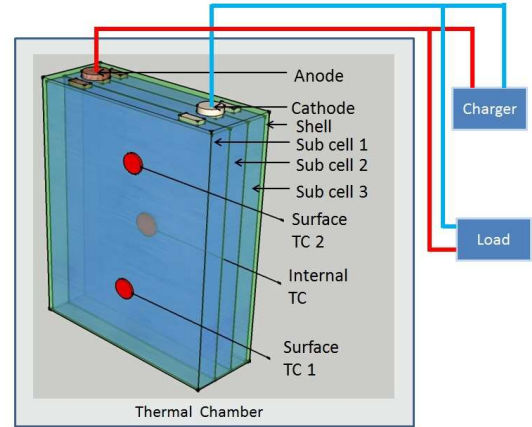

Fig. 2. The battery test system configuration

The battery usable capacity and internal temperature are firstly characterized experimentally at room temperature before and after inserting the thermocouple in order to study whether the inserted thermocouple affects battery performance. The results are shown in Table I, where TC stands for the inserted thermocouple, and 1C and 2C capacity stand for battery usable capacity at 10A and 20A discharging currents. As it can be seen, the effect of the inserted thermocouple on the battery usable capacity (i.e., energy density) and internal resistance (i.e., power density) is negligible. Note that R_i stands for the series internal resistance which does not vary with SOC. Battery usable capacity usually drops when the load current increases. However, according to Table I, the battery usable

capacity increases slightly when the load current varies from 10A to 20A, which is caused by the higher heat generation rate and thus higher battery temperature when the 20A current is applied.

TABLE I
BATTERY CAPACITY AND INTERNAL RESISTANCE TEST

	1C Capacity (Ah)	2C Capacity (Ah)	R_i $(m\Omega)$
Before TC	10.460	10.511	13.5
After TC	10.425	10.433	13.5

Then the battery electrical properties are characterized using the standard hybrid pulse power characterization (HPPC) test as shown in Fig 3 under five different ambient temperatures (i.e., $[0, 10, 23, 39, 52]^\circ C$).
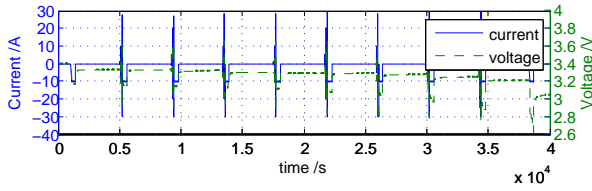

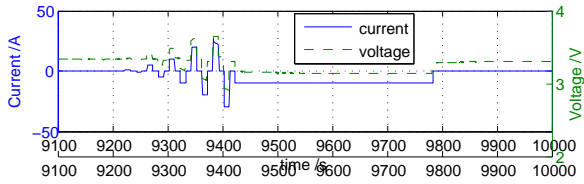Fig. 3. HPPC discharging test under 23 $^\circ C$: terminal current and voltage

Fig. 4. HPPC discharging test under 23 $^\circ C$: one zoomed segment

Besides, two fast discharging tests are run on the battery under $27^\circ C$ ambient temperature, as shown in Fig 5 without forced wind convection and in Fig 6 with forced wind convection, respectively, as a comparison.
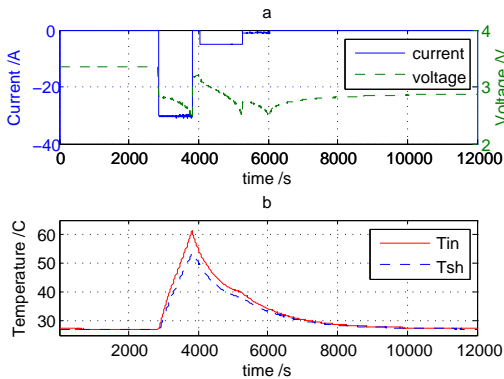

Fig. 5. Battery fast discharging test data without forced wind convection

IV. MODEL IDENTIFICATION

A. Electric submodel identification

Under laboratory test conditions, battery terminal current and voltage can be accurately measured. Then battery SOC can be calculated by current integration method as in Eq (2).
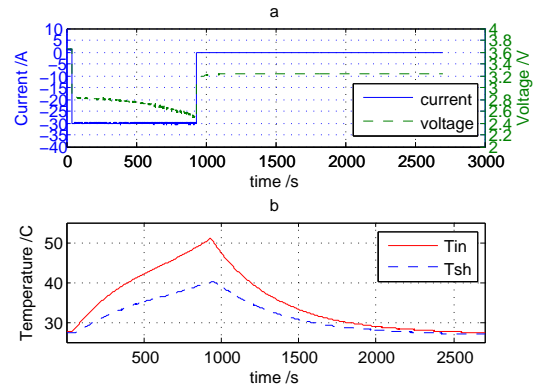

Fig. 6. Battery fast discharging test data with forced wind convection

The same method to determine the battery OCV and hysteresis proposed in [24] is used here. We take the battery voltage after one hour relaxation as the battery charging and discharging OCV, as shown in Fig 7. Their mean value is taken as the battery OCV, and half of the difference between the charging OCV and the discharging OCV is taken as the hysteresis.
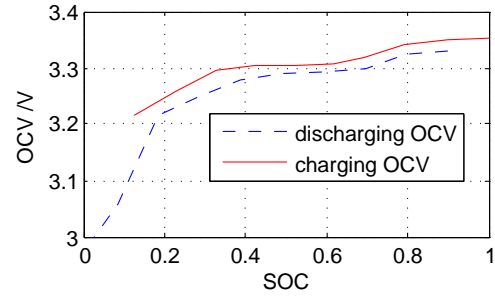

Fig. 7. Battery charging and discharging OCV at 23 $^\circ C$

The other parameters of the electric circuit model are identified by fitting the test data. Note that each test data segment (as shown in Fig 4) is used to identify one set of model parameters at that specific SOC and temperature level. The simulation error minimization method is used in this paper for training the battery electric submodel [25]. To obtain a better model accuracy and stronger consistency, simulation error minimization based model parameter identification methods are preferred over conventional identification methods which minimize the one-step-ahead prediction error in application contexts (e.g., predictive control) where model accuracy is required over a wide horizon [26].

According to Eq (3), the over-potentials across the two RC networks can be calculated as,

$$v_l(k) = a_l^{k-1} v_l(1) + b_l * \sum_{j=1}^{k-1} a_l^{k-1-j} * i(j), \quad l = 1, 2$$

and $V_h(k)$ can be calculated using Eq (4) as follows,

$$V_h(k) = \prod_{j=1}^{k-1} c_j * V_h(1) + M_h * \sum_{m=1}^{k-1} d_m \prod_{j=m+1}^{k-1} c_j$$

Then according to Eq (6), the simulation error is formulated as follows,

$$e(k) = v(k) - f(soc(k)) - V_h(k) - v_1(k) - v_2(k) - R_i * i(k)$$

and the cost function is

$$MSE = \frac{1}{N} \sum_{k=1}^{N} e^2(k) \qquad (11)$$

where N is the length of the test data.

Note that the parameters in the above model include nonlinear ones, e.g., a_l, γ and linear ones, e.g., b_l, M_h, R_i, and the gradient or Hessian information that are needed for parameter optimization are difficult to calculate. Therefore the hybrid parameter optimization method proposed in [24] is adopted in this paper. The nonlinear parameters are optimized by the TLBO method and linear parameters by the least square method. The least square method is nested in the TLBO procedure to reduce the parameter dimension and improve the convergence speed. The details about the hybrid optimization method can be found in [24].

The identified model parameters are shown in Fig 8 to Fig 10. The results reveal that 1) R_i mainly depends on the battery internal temperature (only slight increases at low SOC); 2) R_1, R_2 depend on both the battery SOC and internal temperature; 3) at low SOC level, R_1, R_2 show a noticeable increase in value; 4) the time constant of the R_1C_1 network, $\tau_1 = R_1 * C_1$, depends on the battery SOC. It is clear that, as the temperature increases, the battery internal resistances R_i and R_1, R_2 decrease. The noticeable increase of R_1, R_2 at very low SOC levels (as shown in Fig 9) can be verified by the noticeable voltage drop at low SOC levels (as shown in Fig 3). We can also infer that these varying battery electric parameters will in turn affect the heat generation rate inside the battery based on Eq (7). In summary, the temperature has significant effects on parameters in the battery electric model, which has to be considered in order to improve the modelling and state estimation accuracy.

M_h, γ and $\tau_2 = R_2 * C_2$ are kept constant. $M_h = 0.02; \gamma = 1.5e - 4; \tau_2 = 600$.
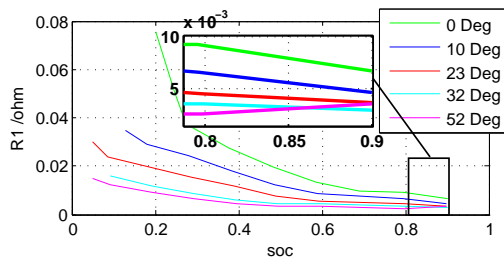
Fig. 8. The electric circuit model parameter identification at different SOC and temperature levels: R_1

Then, part of the electric circuit model identification results are shown in Fig 11. The root mean square error (RMSE) at 80% SOC and 10% SOC are about 3 mV and 10 mV, respectively. At a lower SOC level, the battery shows stronger non-linearity, thus higher modelling error occurs.
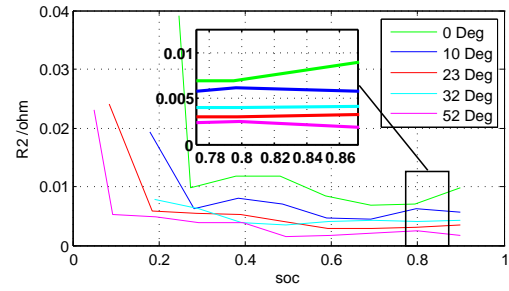
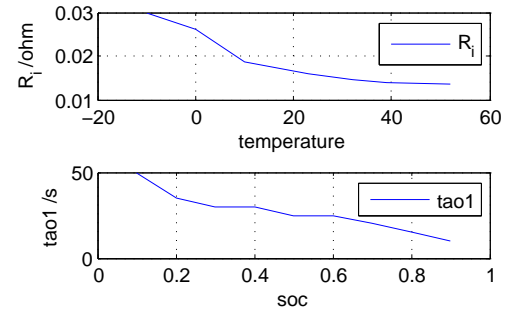Fig. 9. The electric circuit model parameter identification at different SOC and temperature levels: R_2.

Fig. 10. The electric circuit model parameter identification at different SOC and temperature levels: R_i and τ_1.
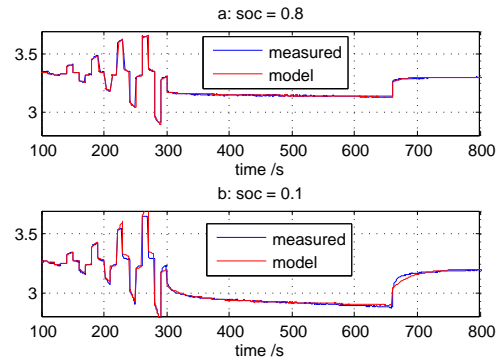
Fig. 11. One part of the electric circuit model identification results at 23 $°C$: (a) at 80% SOC; (b) at 10% SOC.
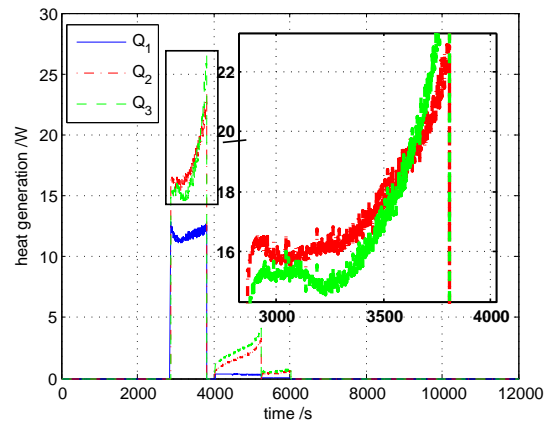
Fig. 12. Three different heat generation calculation methods comparison

B. Thermal submodel identification

The test data shown in Fig 5 (without forced wind convection) is used for thermal model identification. The heat generation results using the three different calculation methods in Eq (7) are compared in Fig 12. The $dOCV/dT_{in}$ values given in [9] is used here. As can be seen, while Q_1 is noticeably smaller than Q_2 and Q_3, the difference between Q_2 and Q_3 is not big (mostly less than 10%). Since the temperature effect on the battery OCV is not considered in this paper, Q_2 is adopted as the heat generation inside the battery.
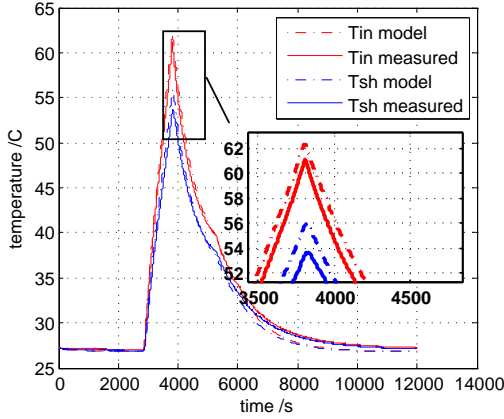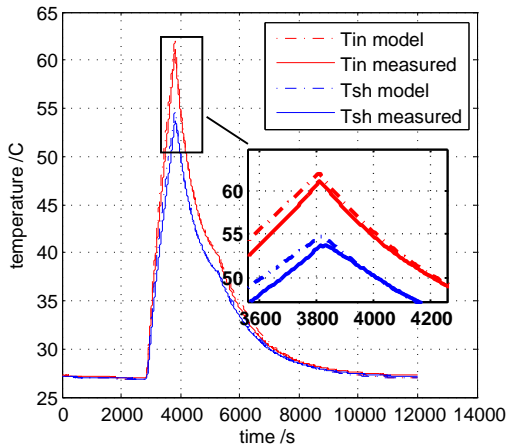

Fig. 13. Thermal modelling results with constant k_2.

Fig. 14. Thermal modelling results with time-varying k_2.

Based on the measured T_{in}, T_{sh}, and the calculated Q_2, Eq (9) can be identified using the least square method.

Note that while we assume that battery thermal properties C_{q1}, k_1, C_{q2} are kept constant (according to [27], battery specific heat capacity is independent of SOC and increases slightly with temperature; battery cross-plane thermal conductivity is independent of temperature but depends on SOC.), k_2 certainly depends on the heat dissipation condition, such as cooling wind speed and temperature. According to [23], k_2 also increases with this temperature gradient $T_{sh} - T_{amb}$. To take this effect into consideration, two cases are compared

Modelling Results	T_{in} max error	T_{in} RMSE	T_{sh} max error	T_{sh} RMSE
constant k_2	1.51	0.695	2.31	0.714
varying k_2	0.90	0.469	1.02	0.467

here: 1) constant k_2; 2) time-varying k_2, i.e., $k_2 = k_{2,1} + k_{2,2} * (T_{sh} - T_{amb})$.
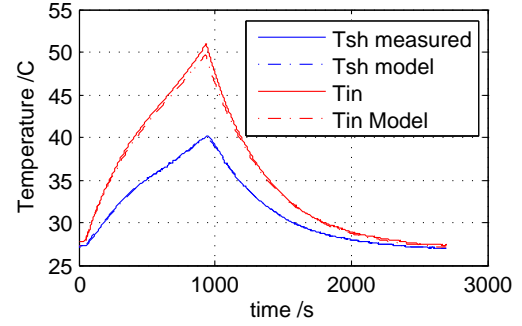

Fig. 15. Kalman filter results assuming constant electrical submodel parameters: T_{in}, T_{sh}
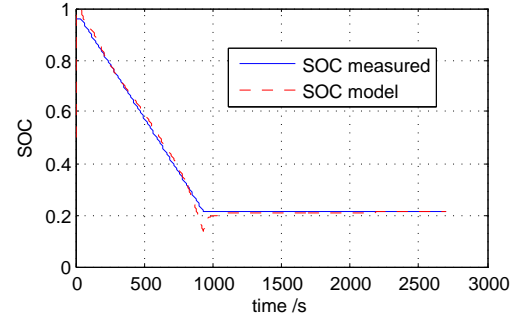
Fig. 16. Kalman filter results assuming constant electrical submodel parameters: SOC

The thermal modelling results are shown in Fig 13 for constant k_2 and Fig 14 for time-varying k_2, respectively. The modelling results are summarized in Table II. As shown, when the time-varying nature of k_2 is taken into consideration, the model accuracy is improved noticeably.

Finally, the identified battery thermal model parameters are

$$C_{q1} = 288.77, \ C_{q2} = 30.8,$$
$$k_1 = 1.7312, \ k_{2,1} = 0.3205, \ k_{2,2} = 0.0028 \quad (12)$$

V. KALMAN FILTER

After the battery model is identified, it can be used for battery internal states estimation. Note that in Eq (10), battery behaviour is described using a state-space equation. Therefore, the popular EKF method can be used for the states estimation.

As discussed above, k_2 depends on the heat dissipation condition. To deal with this, one approach would be to characterize k_2 off-line under different operation conditions and tabulate the results. The tabular can then be used for

realtime applications. However, to build such a table requires many running tests which is time consuming. In this paper, an joint EKF is adopted to simultaneously estimate both the model states (x in Eq (10)) and time-varying model parameter (k_2) in realtime [13], [24].

Take k_2 as another model state, and the augmented model state equations become,

$$x_a(k) = A_a(k-1) * x(k-1) + B_a(k-1) \quad (13)$$

where

$$x_a(k) = [x(k); k_2(k)]$$

$$A_a(k-1) = blkdiag(A(k-1), 1)$$

$$B_a(k-1) = [B(k-1); 0]$$

Then k_2 can be estimated along with other model states.

A detailed implementation procedure of the joint EKF method can be found in [13], [24].

The battery fast discharging test data with forced wind convection shown in Fig 6 are used for validation of the proposed internal states estimation method. In order to demonstrate that it is important to consider the couplings between battery thermal and electrical behaviours, two different scenarios are considered and compared, one assuming constant battery model parameters and the other considering the interactions. The system states, i.e., x_a in Eq (13) which includes both electrical states (i.e., battery SOC, over-potentials across RC networks, and hysteresis voltage), and thermal states (i.e., internal temperature and surface temperature), and time-varying model parameter (i.e., heat dissipation level k_2), are estimated in both cases.

A. KF results based on the electrical submodel with constant parameters

The values of the constant parameters in the model are given as follows

$$\tau_1 = 15s; \; R_1 = 8m\Omega; \; R_2 = 6m\Omega \quad (14)$$

which are approximated with the corresponding mean values.

The Kalman filter estimation results are shown in Fig 15 and Fig 16. It is clear that the estimated battery internal temperature matches well with the measurements during the whole testing period. The maximum error and RMSE of T_{in} estimation are only about $1.48°C$ and $0.44°C$, respectively. The SOC estimation RMSE is 2.88%.

Since the battery shell temperature is directly measurable, the estimated T_{sh} results match the measurements perfectly.

The model voltage output is shown in Fig 17, where two short segments with slight bias error can be observed at both the starting and ending stages (around 100s and 900s, respectively). We believe the bias errors are caused by the discrepancy between the adopted constant battery model parameters in Eq (14) and the time-varying true model parameters shown in Fig 8 to Fig 10.
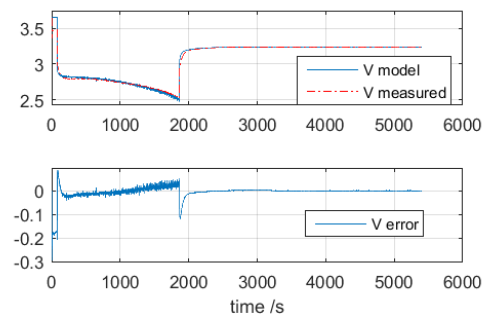

Fig. 17. Kalman filter results assuming constant electrical submodel parameters: battery terminal voltage

B. KF results considering the T_{in} and SOC effect on model parameters

The Kalman filter results considering T_{in} and SOC effects are shown in Fig 18 to Fig 20. As it is shown, the internal temperature estimation results in Fig 18 are quite similar to Fig 15. The reason is that in these two scenarios the thermal submodels used are the same. The maximum error and RMSE of T_{in} estimation are only about $1.2°C$ and $0.47°C$, respectively. These estimation results are comparable with existing results [8], [23], [28], where the RMSE errors lie between 0.5 and $2°C$.

The battery SOC estimation results are shown in Fig 19. As can be seen, the estimated battery SOC converges to the correct value quickly. The SOC estimation RMSE value is 2.31%, about 20% improvement compared with that in Fig 16. It is evident that the SOC estimation accuracy in Fig 19 is higher than Fig 16 during the whole test period.
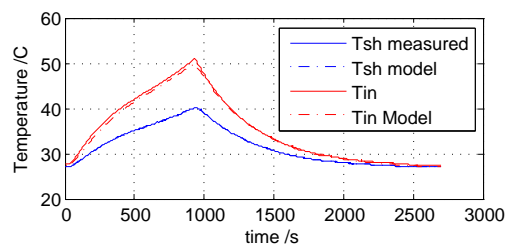

Fig. 18. Kalman filter considering T_{in} and SOC effect on the model parameters: T_{in}, T_{sh}.

The estimation results of the time-varying model parameter k_2 are shown in Fig 20. The initial value of k_2 is set to be 0.3. As can be seen, the estimated k_2 quickly increased to a much higher value (i.e., 1.3). After the discharging test ended, k_2 converged to a stable value (i.e., 1.2). Comparing this result with Eq (12), we can conclude that the forced wind convection increased k_2 noticeably from less than 0.4 to 1.2.

During this test, the electrical submodel parameters change with the battery T_{in} and SOC, and the results are shown in Fig 21. As can be seen, the value of R_1 started from about $4m\Omega$ and increased to over $15m\Omega$, while the value of R_2 increased from $4m\Omega$ to about $7m\Omega$. Consequently, the over-potentials v_1 and v_2 changed dramatically as the discharging test went

on. If this effect is not captured, the modelling accuracy will be significantly reduced.
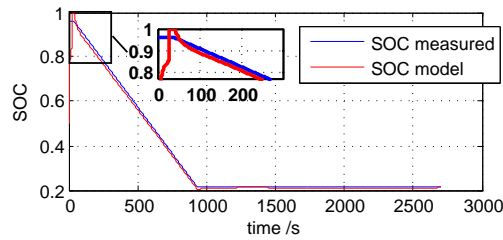

Fig. 19. Kalman filter considering T_{in} and SOC effect on the model parameters: SOC.
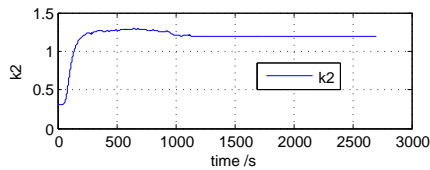

Fig. 20. Kalman filter considering T_{in} and SOC effect on the model parameters: k_2.

Note that the battery internal resistance R_1, R_2 normally will drop as the battery internal temperature increases. However, in this fast discharging test, the battery SOC dropped too fast and became the dominant factor to increase the internal resistance. If the battery is heated up at the same SOC, the decrease of R_1, R_2 becomes more noticeable.
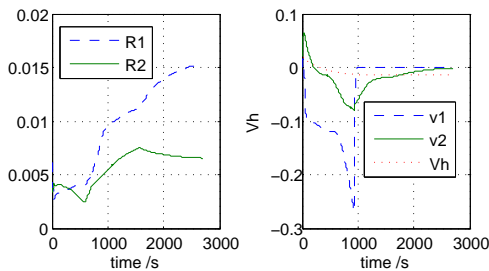

Fig. 21. Kalman filter results considering T_{in} and SOC effect on the model parameters: electrical submodel parameters R_1, R_2 and over-potentials v_1, v_2, V_h.

The battery terminal voltage fitting results are shown in Fig 22. As can be seen, the model outputs match very well with the measurements, except for a few error spikes.

Generally speaking, the state estimation performance of EKF depends not only on the model accuracy, but also on the choice of EKF parameters. According to the above analysis and experimental results, we conclude that a better model can significantly improve the state estimation accuracy. This has been achieved through capturing the effect of SOC and T_{in} on the battery behaviours using the coupled thermoelectric model. It should be noted that some other remedies to improve the internal state estimation accuracy have also been proposed, such as Dual-Kalman Filter method, RLS + EKF, etc. These approaches however can only be more effective with a more
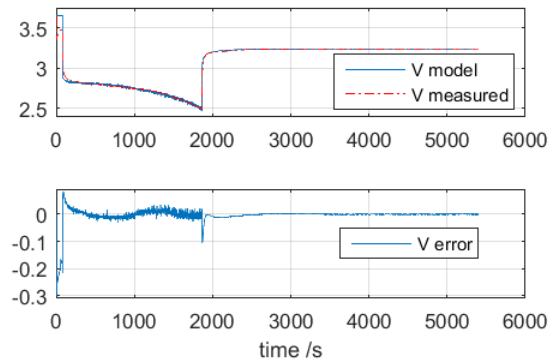

Fig. 22. Kalman filter results considering T_{in} and SOC effect on the model parameters: battery terminal voltage.

accurate model as we have proposed in this paper. It is also worth noting that due to the higher model accuracy by considering the interactions between the battery thermal and electrical behaviours, the EKF parameter tuning used in this study is much easier. To compare these different approaches is beyond the scope of this paper, and it can be a future work.

VI. CONCLUSIONS

A novel method is proposed in this paper to estimate battery internal temperature and SOC simultaneously. A simplified thermoelectric model is built, including an electrical submodel and a thermal submodel. For the thermal submodel, different methods for calculating the heat generation inside the battery are compared; for the electrical submodel, the effect of battery internal temperature and SOC on the battery electrical behaviours is characterized and captured. The time-varying thermal submodel parameter is also taken into consideration, and a joint EKF is applied to estimate the model states and time-varying model parameter simultaneously. The proposed estimation method is based only on the online measurable signals, e.g., battery voltage, current and shell temperature, and thus can be implemented in realtime. Test data are collected using a LiFePO$_4$ battery. The modelling and internal temperature and SOC estimation results has confirmed the efficacy of the proposed method.

Future work to further improve the model accuracy may consider the following three aspects: 1) variations of thermal and electric behaviours between cells within a battery pack; 2) battery ageing and usable capacity reduction with cycling usage; 3) the temperature effect on battery OCV.

REFERENCES

[1] L. Lu, X. Han, J. Li, J. Hua, and M. Ouyang, "A review on the key issues for lithium-ion battery management in electric vehicles," *Journal of Power Sources*, vol. 226, pp. 272–288, Mar. 2013.

[2] R. R. Richardson, P. T. Ireland, and D. A. Howey, "Battery internal temperature estimation by combined impedance and surface temperature measurement," *Journal of Power Sources*, vol. 265, pp. 254–261, Nov. 2014.

[3] C. G. Motloch, J. P. Christophersen, J. R. Belt, R. B. Wright, G. L. Hunt, R. A. Sutula, T. Duong, T. J. Tartamella, H. J. Haskins, and T. J. Miller, "High-power battery testing procedures and analytical methodologies for HEV's," SAE Technical Paper, Tech. Rep., Jun. 2002.

[4] G.-H. Kim, A. Pesaran, and R. Spotnitz, "A three-dimensional thermal abuse model for lithium-ion cells," *Journal of Power Sources*, vol. 170, no. 2, pp. 476–489, Jul. 2007.

[5] G. Guo, B. Long, B. Cheng, S. Zhou, P. Xu, and B. Cao, "Three-dimensional thermal finite element modeling of lithium-ion battery in thermal abuse application," *Journal of Power Sources*, vol. 195, no. 8, pp. 2393–2398, Apr. 2010.

[6] K. Smith, G.-H. Kim, E. Darcy, and A. Pesaran, "Thermal/electrical modeling for abuse-tolerant design of lithium ion modules," *International Journal of Energy Research*, vol. 34, no. 2, pp. 204–215, Feb. 2010.

[7] Y. Xiao and B. Fahimi, "State-space based multi-nodes thermal model for lithium-ion battery," in *Transportation Electrification Conference and Expo (ITEC), 2014 IEEE*. IEEE, Jun. 2014, pp. 1–7.

[8] X. Lin, H. E. Perez, J. B. Siegel, A. G. Stefanopoulou, Y. Li, R. D. Anderson, Y. Ding, and M. P. Castanier, "Online parameterization of lumped thermal dynamics in cylindrical lithium ion batteries for core temperature estimation and health monitoring," *IEEE Trans. Control Syst. Technol.*, vol. 21, no. 5, pp. 1745–1755, Sep. 2013.

[9] J. Sun, G. Wei, L. Pei, R. Lu, K. Song, C. Wu, and C. Zhu, "Online internal temperature estimation for lithium-ion batteries based on kalman filter," *Energies*, vol. 8, no. 5, pp. 4400–4415, May. 2015.

[10] S. Piller, M. Perrin, and A. Jossen, "Methods for state-of-charge determination and their applications," *Journal of Power Sources*, vol. 96, no. 1, pp. 113–120, Jun. 2001.

[11] W. Chang, "The state of charge estimating methods for battery: a review," *ISRN Applied Mathematics*, vol. 2013, Jul. 2013.

[12] N. Watrin, B. Blunier, and A. Miraoui, "Review of adaptive systems for lithium batteries state-of-charge and state-of-health estimation," in *Transportation Electrification Conference and Expo (ITEC)*. IEEE, Jun. 2012, pp. 1–6.

[13] G. L. Plett, "Extended kalman filtering for battery management systems of lipb-based hev battery packs: Part 3. state and parameter estimation," *Journal of Power Sources*, vol. 134, no. 2, pp. 277–292, Aug. 2004.

[14] G. L. Plett, "Sigma-point kalman filtering for battery management systems of lipb-based hev battery packs: Part 1: Introduction and state estimation," *Journal of Power Sources*, vol. 161, no. 2, pp. 1356–1368, Oct. 2006.

[15] W. Gu and C. Wang, "Thermal-electrochemical modeling of battery systems," *Journal of The Electrochemical Society*, vol. 147, no. 8, pp. 2910–2922, Aug. 2000.

[16] V. Srinivasan and C. Wang, "Analysis of electrochemical and thermal behavior of li-ion cells," *Journal of The Electrochemical Society*, vol. 150, no. 1, pp. A98–A106, Jan. 2003.

[17] M.-H. Chang, H.-P. Huang, and S.-W. Chang, "A new state of charge estimation method for lifepo4 battery packs used in robots," *Energies*, vol. 6, no. 4, pp. 2007–2030, Apr. 2013.

[18] F. Baronti, G. Fantechi, L. Fanucci, E. Leonardi, R. Roncella, R. Saletti, and S. Saponara, "State-of-charge estimation enhancing of lithium batteries through a temperature-dependent cell model," in *Applied Electronics (AE), 2011 International Conference on*. IEEE, Sep. 2011, pp. 1–5.

[19] Y. Xing, W. He, M. Pecht, and K. L. Tsui, "State of charge estimation of lithium-ion batteries using the open-circuit voltage at various ambient temperatures," *Applied Energy*, vol. 113, pp. 106–115, Jan. 2014.

[20] C. Zhang, K. Li, and J. Deng, "Real-time estimation of battery internal temperature based on a simplified thermoelectric model," *Journal of Power Sources*, vol. 302, pp. 146–154, Jan. 2016.

[21] C. Zhang, K. Li, S. Mcloone, and Z. Yang, "Battery modelling methods for electric vehicles - a review," in *Control Conference (ECC), 2014 European*. IEEE, Jun. 2014, pp. 2673–2678.

[22] BestgoPower, "Lifepo4 battery temperatures test," Access date: Jun 2014. [Online]. Available: http://www.bestgopower.com/technology/documents/temperature-test.html

[23] H. Dai, L. Zhu, J. Zhu, X. Wei, and Z. Sun, "Adaptive kalman filtering based internal temperature estimation with an equivalent electrical network thermal model for hard-cased batteries," *Journal of Power Sources*, vol. 293, pp. 351–365, Oct. 2015.

[24] C. Zhang, K. Li, L. Pei, and C. Zhu, "An integrated approach for real-time model-based state-of-charge estimation of lithium-ion batteries," *Journal of Power Sources*, vol. 283, pp. 24–36, Jun. 2015.

[25] C. Zhang, K. Li, Z. Yang, L. Pei, and C. Zhu, "A new battery modelling method based on simulation error minimization," in *PES General Meeting— Conference & Exposition, 2014 IEEE*. IEEE, Jul. 2014, pp. 1–5.

[26] M. Farina and L. Piroddi, "Some convergence properties of multi-step prediction error identification criteria," in *Decision and Control, 2008. CDC 2008. 47th IEEE Conference on*. IEEE, Dec. 2008, pp. 756–761.

[27] S. J. Bazinski and X. Wang, "Experimental study on the influence of temperature and state-of-charge on the thermophysical properties of an lfp pouch cell," *Journal of Power Sources*, vol. 293, pp. 283–291, Oct. 2015.

[28] F. Sun, X. Hu, Y. Zou, and S. Li, "Adaptive unscented kalman filtering for state of charge estimation of a lithium-ion battery for electric vehicles," *Energy*, vol. 36, no. 5, pp. 3531–3540, May. 2011.

Cheng Zhang received the B.Sc. and M.Sc. degree in Control Science and Engineering from Harbin Institute of Technology, Harbin, China, in 2010 and 2012, respectively, and the Ph.D. degree in Electrical Electronics Engineering from Queen's University Belfast, Belfast, in 2016.

He is now working at WMG, University of Warwick as a research fellow. His research interests include battery management system, battery modelling and state estimation.

Kang Li (M05, SM11) received his Ph.D. degree in Control Theory and Applications from Shanghai Jiaotong University, Shanghai, China, in 1995, and D.Sc. degree in Engineering from Queen's University Belfast, UK, 2015.

He is a Chair Professor with the School of Electronics, Electrical Engineering and Computer Science, Queen's University Belfast, UK.

His research interests include nonlinear system modelling, identification, and control, and bio-inspired computational intelligence, with applications to the development of advanced control technologies for decarbonizing the whole energy systems, from integration of renewable energies, smart grid, to electric vehicles, and energy reduction in manufacturing. He is developing a new generation of minimal-invasive energy monitoring system and intelligent control platform which are currently trialled in several energy intensive industries.

Jing Deng received his Ph.D. degree from the Intelligent Systems and Control(ISAC) Group at Queen's University Belfast,UK in 2011.

He is currently a research fellow at Energy, Power, and intelligent control cluster, Queen's University Belfast. His research interests include system modelling, pattern recognition and fault detection, and fuzzy control, and internet of things with applications on intelligent manufacturing, energy saving, and industry 4.0.

Shiji Song received the Ph.D. degree from the Department of Mathematics, Harbin Institute of Technology, Harbin, China, in 1996.

He is currently a Professor with the Department of Automation, Tsinghua University, Beijing, China.

His current research interests include system modeling, control and optimization, computational intelligence, and pattern recognition.